ADVANCED ENGINEERING MATERIALS

DOI: 10.1002/adem.201300146

Small-Scale Deformation of Pulsed Electric Current Sintered Silicon Oxycarbide Polymer Derived Ceramics

By *Ravindran Sujith, Nedunchezhian Srinivasan* and *Ravi Kumar**

The deformation behavior of pulsed electric current sintered silicon oxycarbide ceramics produced by the solid-state thermolysis of polyhydridomethylsiloxane at small-scale is investigated. The ceramics remained X-ray amorphous after sintering at 1300 °C in vacuum and a high density of ≈2.35 g cm^{-3} is achieved. The elastic constants of these ceramics are determined using non-destructive ultrasonic testing method. The elasto-plastic deformation under contact loading is determined using depth sensing nanoindentation technique. An indentation hardness of ≈11 GPa and reduced elastic modulus of ≈105 GPa is observed. The load–displacement curves display significant elastic recovery with an elastic work ratio of ≈0.71. The evolution of Hertzian cone cracks upon microindentation indicates an anomalous deformation behavior.

Silicon oxycarbide (SiOC) ceramics synthesized through polymer derived ceramic (PDC) route are widely considered for a variety of high-end applications such as ceramic glow plugs, thermal protection for re-entry space vehicles, and microelectromechanical systems (MEMS).[1,2] However, continuous evolution of volatile matter during solid state thermolysis often resulted in a porous ceramic. Though the porosity generated can be controlled effectively to meet specific applications such as in gas separation filters,[3,4] lack of a relatively dense structure makes it extremely difficult to precisely estimate the mechanical properties. Nevertheless, near-dense PDCs were produced by cast route in which shaping was carried out at the precursor stage.[5,6] However, its application is limited to the production of thin ceramics, since these ceramics were observed to crack at larger thicknesses due to the stresses developed by the compelling need for the evolution of gases. An alternative method to obtain a relatively dense structure is to shape the ceramic after thermolysis. Hot pressing and pulsed electric current sintering (PECS) more commonly known as spark plasma sintering (SPS) are the two common techniques where shaping is done after thermolysis.[1] In comparison to hot pressing, PECS gained interest because of its ability to produce high-dense materials in short processing time by the simultaneous application of pulsed current at high amperage, high heating rates and pressures.[7–9]

PECS for the production of PDCs with high achievable densities was reported for the first time by Wan *et al*.[10] wherein dense pellets of SiC–Si_3N_4 nanocomposites were produced with yttria as an additive. However, there is rather limited literature available on the PECS of SiOC PDCs.[11,12] For instance, the microstructural evolution of dense SiOC ceramics sintered up to 1600 °C with a hardness of ≈7 GPa and flexural strength of ≈220 MPa was reported by Esfehanian *et al*.[11] Furthermore, the influence of applied pressure during PECS on the structural and microstructural evolution of SiOC ceramics was reported by Mazo *et al*. Moreover, the same authors have also reported a thermal conductivity value of ≈1.38 Wm^{-1} K^{-1} which were found to remain independent of the processing parameters used.[12] Despite these aforementioned studies, a comprehensive understanding of the elasto-plastic response and the underlying deformation mechanisms of these PECS ceramics is hitherto not been investigated. Hence, the focus of the present study is on the determination of the mechanical properties of PECS SiOC ceramics at small-scales using an instrumented indentation technique. Owing to the inherent brittle nature of these ceramics, instrumented indentation stands out as an ideal technique to capture the elasto-plastic response of these materials. To achieve this, micro- and nanoindentation experiments were performed. Furthermore, the deformation mechanisms were understood by analyzing the evolution of crack patterns under contact loading at various loads and were compared with the respective crack evolution patterns observed in fused quartz. Henceforth, a non-destructive ultrasonic frequency testing method was adopted to evaluate the elastic constants such as

[*] *Dr. R. Kumar, R. Sujith, N. Srinivasan*
Materials Processing Section, Department of Metallurgical and Materials Engineering, Indian Institute of Technology Madras, Chennai 600036, India
E-mail: nvrk@iitm.ac.in

[**] *We gratefully acknowledge the Center for Non-Destructive Evaluation (CNDE), Indian Institute of Technology Madras for providing access to ultrasonic non-destructive testing.*

shear modulus, bulk modulus, elastic modulus, and Poisson's ratio.

1. Materials and Experimental Methods

A commercially available polyhydridomethylsiloxane procured from Sigma–Aldrich, India, (CAS Number-63148-57-2) with chemical formula $(CH_3)_3$–Si(O)–$[CH_3(H)Si–O]_n$-$Si(CH_3)_3$ (average M_n: 1700–3200, viscosity:15–40 mPa s) was used as the polymeric precursor to synthesis SiOC powder. The polymer was initially crosslinked at room temperature by the addition of 5 wt% of 1,4-diazabicyclo [2.2.2] octane (Sigma–Aldrich, India). This cross-linking agent was used because it is inexpensive when compared to vinyl based agent and platinum catalyst reported in the literature.[13,14] The cross-linked polymer was subsequently thermolysed in an alumina tubular furnace at 1000 °C for 2 h in Ar atmosphere at a heating rate of 5 °C min^{-1}. The elemental composition of the as-thermolysed SiOC powder derived from polyhydridomethylsiloxane was considered identical to the reported composition by Blum *et al*.[14] Henceforth, the as-thermolysed ceramic was ground to fine powder using an agate mortar and pestle. The ground powder was sieved through a sieve shaker machine and powder particles >125 μm in size were selected for consolidation. The powder was taken in 20 mm graphite die and the sintering was carried out using a pulsed electric sintering machine (Sumitomo Coal Mining Co. Ltd, Japan) in vacuum. The machine is capable of working at a maximum current and voltage of 3000 A and 15 V, respectively. The graphite foils were placed between the powder and the die in order to prevent sticking between the two. PECS was carried out at maximum load of 30 MPa and at sintering temperatures of 1300 and 1500 °C maintaining a heating rate of 100 °C min^{-1} and holding time of 15 min. The PECS samples processed at 1300 and 1500 °C, will hereafter be referred to as SiOC1300 and SiOC1500, respectively.

The crystallization behavior was investigated by X-ray diffraction (D8 Discover, AXS X-ray diffractometer, USA), using Cu Kα radiation ($\lambda = 0.15408$ nm) in the 5 to 90°, 2θ range. The apparent density of the sample was determined by the water displacement method. The experiment was repeated three times and the average with standard deviation was mentioned. The indentation hardness and the reduced elastic modulus were determined using a depth-sensing nano-indenter (Hysitron Inc., USA) operated at room temperature. A Berkovich indenter was used for all the measurements and five different loads ranging from 2 to 10 mN were chosen. The following trapezoidal loading sequence was chosen for each of the load sets: 10 s for loading, 10 s for holding and 10 s for unloading. For each load set, 10 indentations were taken and the average with the standard deviation was reported. The imaging of the nanoindentation was done using an in situ scanning probe microscopy (SPM) imaging technique. The indenter tip area was calibrated by performing a set of 25 indents on a standard fused quartz sample supplied by Hysitron Inc. For loads between 1.96 and 9.8 N, a standard Vickers pyramidal microindentor (Wolpert Wilson 4325VA) was used. Five indentations were taken and for each load a holding time of 10 s was provided. The average of the five values along with standard deviation was provided. The samples for the indentation studies were polished with different grades of emery paper, followed by diamond polish (0.25 μm) to achieve a mirror finish. The images of the microindentation were taken using an in situ optical microscope attached to the microindenter. The elastic constants were determined by an ultrasonic non-destructive evaluation technique. A pulser-receiver (5900 PR) of frequency range from 200 kHz to 200 MHz was used. Ultrasonic velocities were measured using 10 MHz longitudinal wave and 5 MHz shear wave transducers.

2. Results and Discussion

The apparent densities of SiOC1300 and SiOC1500 ceramics are ≈2.35 and 2.30 g cm^{-3}, respectively (Table 1). This suggests that the maximum densification was achieved at a sintering temperature of 1300 °C and with further increase in temperature to 1500 °C a marginal drop (≈2%) in the density value was observed. This corresponding decrease in the density value from SiOC1300 to SiOC1500 could be attributed to the carbothermal reduction of SiOC leading to the formation of microporosity. Similar trend in the reduction of density value from 2.46 to 2.35 g cm^{-3} for the SiOC ceramics sintered at 1300 and 1500 °C was reported by Mazo *et al*.[12] In the PECS technique, the densification is expected to occur due to the conductive and radiative heat transfer from the die to the powder, whilst the die and punches are heated as per Joule heating derived from the pulsed electric current. However, the contributions to densification due to the current flow through the SiOC ceramic could be considered insignificant since the electrical conductivity of these ceramics are minimal.

The room temperature XRD of the PECS SiOC ceramics is shown in Figure 1. The SiOC1300 ceramic was observed to remain X-ray amorphous, in contrast to SiOC1500 ceramic, which exhibited phase separation. The broad peaks observed at $2\theta = 35.5$, 60, and 72° were assigned to β-SiC (PDF #892640)

Table 1. Elastic constants of PECS SiOC ceramics determined by non-destructive ultrasonic testing.

Sample	Apparent density (g cc^{-1})	Thickness (mm)	V_l (m s^{-1})	V_t (m s^{-1})	ν	E (GPa)	G (GPa)	K (GPa)
SiOC1300	2.35 ± 0.01	2.90	6613	4050	0.21	91.30	38.54	51.38
SiOC1500	2.30 ± 0.01	4.32	6565	3950	0.22	86.82	35.89	51.28

ADVANCED ENGINEERING MATERIALS 2013,
DOI: 10.1002/adem.201300146

ADVANCED ENGINEERING MATERIALS

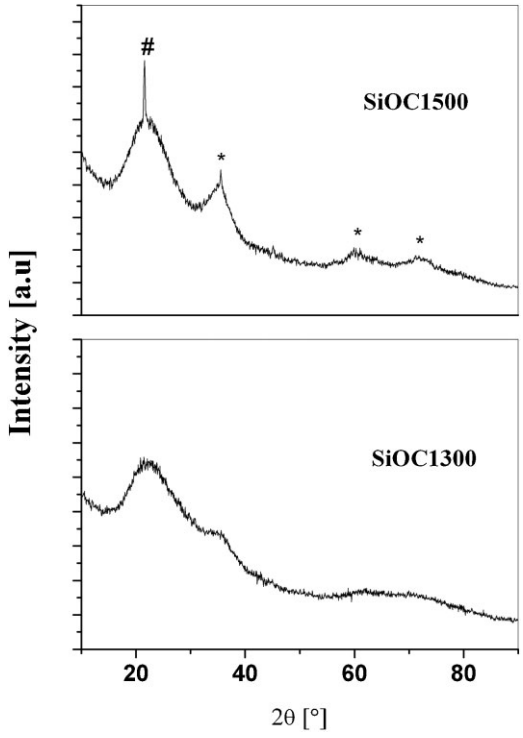

Fig. 1. X-ray diffractograms of the PECS SiOC ceramics: ∗, SiC; #, SiO_2.

and the sharp peak at $2\theta = 22°$ was attributed to crystobalite (PDF #893606). The phase separation of SiOC into thermodynamically stable phases of SiC and SiO_2 at temperature higher than 1450 °C was reported in the literature.[12,14] The crystallite size of β-SiC was calculated using Scherrer's formula and was ~3 nm suggesting insignificant crystallite coarsening. Limited crystallite growth of SiC has been reported earlier and was primarily attributed to limited diffusivity of Si and C atoms due to the high viscosity of SiOC.[11,15] However, Rouxel *et al.*[16] have reported that the viscosity of SiOC tends to drop from $\sim 10^{16}$ to 10^{12} Pa s upon an increase in temperature from 1000 to 1500 °C. Since the viscosity value is relatively low ($\sim 10^{12}$ Pa s) at temperatures of 1500 °C, the influence of viscosity on the crystallite growth of SiC could be considered insignificant. Nevertheless, it is important to note that significantly higher heating rates and lower holding times were adopted in PECS and the resulting limited diffusion kinetics could have attributed to the restricted crystallite growth of SiC.

The calculated values of longitudinal (V_l) and transverse (V_t) velocities for SiOC1300 and SiOC1500 are shown in the Table 1. The elastic constants were computed from the velocities using the following empirical relations.[17]

$$\nu = \frac{V_l^2 - 2V_t^2}{2V_l^2 - 2V_t^2} \tag{1}$$

$$E = \frac{V_l^2 \rho(1+\nu)(1-2\nu)}{(1-\nu)} \tag{2}$$

$$G = V_t^2 \rho \tag{3}$$

where, υ is the Poisson's ratio, E is the Young's modulus in GPa, G is the shear modulus in GPa, and K is the bulk modulus in GPa. The Poisson's ratio of these ceramics is ≈0.21 (Table 1) and the glasses were observed to have a ν-value between 0.11 and 0.30.[18] However, it should be noted that only limited number of studies were carried out in PDCs on the estimation of Poisson's ratio.[19–21] For instance, ν of SiOC ceramic (produced by warm pressing) was reported only once wherein a very low value of 0.11 was reported.[19] In addition, similar studies on SiCN ceramics produced by cast route ($\nu = 0.22$)[20] and for the HfO_2/SiCN(O) ceramic nanocomposite produced by PECS ($\nu \approx 0.22$)[21] were also reported. However, the higher value of ν for the Si–O–C ceramics produced by PECS route compared to the warm pressed SiOC ceramic could be due to the difference in the processing routes. Moreover, the elastic constants were marginally higher for the SiOC1300 in contrast to SiOC1500 (≈5%) which could be attributed to the effect of phase separation and presence of nanoclusters in the phase separated ceramic.[22] Furthermore, this could be correlated to the increase in Poisson's ratio (0.21–0.22) inferring SiOC1500 was comparatively less stiffer than SiOC1300. In addition, the Pugh ratio (G/K)[23] which can be considered as the measure of elasticity was ≈0.75, suggesting the brittle behavior of these ceramics.

An exemplary illustration of the load–displacement curve of SiOC1500 ceramic subjected to nanoindentation at varied loads between 2 and 10 mN (P_{max}) is shown in Figure 2. The curves were analyzed using Oliver and Pharr method.[24,25] The final indentation depths (h_f) and the maximum indentation depths (h_{max}) were deduced from the plot. The unloading segment of the curve was fitted using the power law relation,

$$P = B(h - h_f)^m \tag{4}$$

where, P is the load in mN, h is the displacement in nm and B and m are the fitting parameters. The power law index (m) was

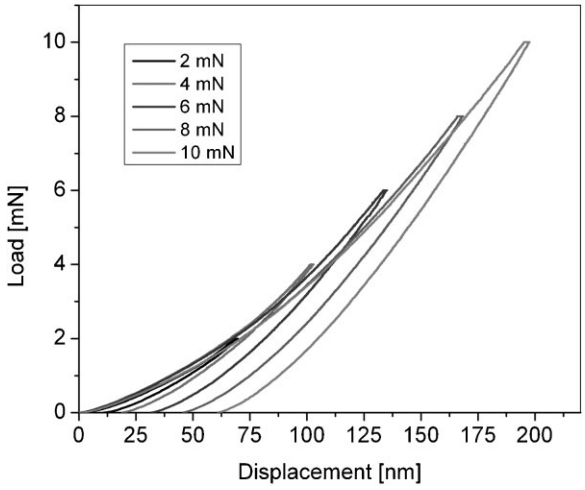

Fig. 2. Load–displacement curves for SiCO1500 subjected to indentation at varied loads between 2 and 10 mN.

DOI: 10.1002/adem.201300146

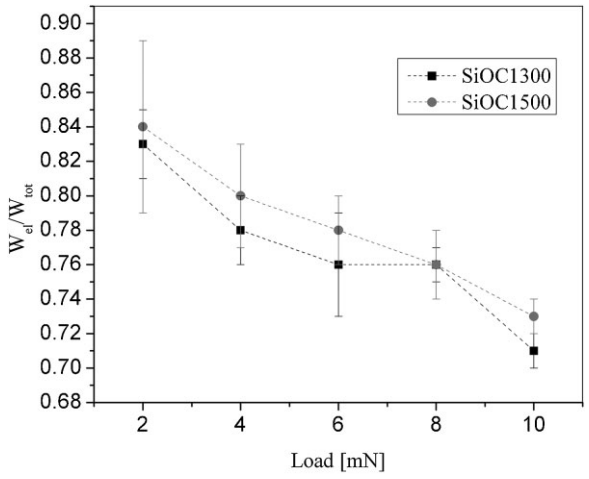

Fig. 3. The evolution of elastic work ratio with indentation load.

≈1.5 and was comparable to the value reported for other PDCs.[21]The residual depth ratio (h_f/h_{max}) determined from the load–displacement curves for these ceramics was 0.31 ± 0.02 at a P_{max} of 10 mN (SiOC1500), indicating considerable elastic recovery upon unloading. This high elastic recovery can be considered as a characteristic feature of these PDCs.[19,20,26] Moreover, a similar residual depth ratio (0.31 ± 0.01) was observed for the fused quartz sample at a P_{max} of 10 mN. However, at lower loads the h_f/h_{max} was observed to decrease to 0.21 ± 0.01, inferring the recovery was more pronounced at lower loads. This suggests that the mechanisms responsible for plastic deformation were not fully activated at lower loads, thereby resulting in an increased elastic recovery. A similar behavior was reported for glassy carbons, wherein at loads below a critical value the indentations were fully recovered.[27]

The ratio of work done during elastic deformation (W_{el}) to the total work done (W_{tot}) during indentation (W_{el}/W_{tot}) is an important parameter, which is widely being used to understand the elasto-plastic deformation involved during indentation. These are the parameters, which can be readily obtained from the load–displacement curve and is closely related to the plasticity index. W_{el}/W_{tot} tends to 1 and 0 for a perfectly elastic and plastic material, respectively. The variation of W_{el}/W_{tot} with indentation load for SiOC1300 and SiOC1500 is shown in Figure 3 and it can be inferred that W_{el}/W_{tot} is >0.5 for SiOC1300 and SiOC1500 ceramics. For materials with $W_{el}/W_{tot} > 0.5$ pile-ups were observed to be insignificant.[28] This can be further corroborated from the SPM (Figure 4) inferring no appreciable pile-up around the indication. Hence, the influence of pile-ups on the hardness determined by the Oliver-Pharr method can be neglected. Moreover, at lower indentation loads, W_{el}/W_{tot} was observed to increase inferring the plastic contribution to the total work done is insignificant at lower loads. W_{el}/W_{tot} of SiOC1300, SiOC1500 and fused quartz at a P_{max} of 10 mN are provided in Table 2. Interestingly, W_{el}/W_{tot} of SiOC ceramics produced by PECS and fused quartz were similar, suggesting the deformation behavior of both to be the same, at the load regimes considered.

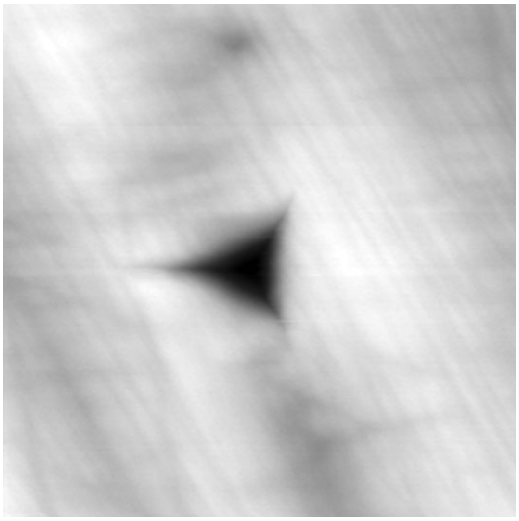

Fig. 4. Scanning probe micrograph of the indent on SiOC1500 at a P_{max} of 10 mN (image size: 4 μm × 4 μm).

The contact stiffness (S) at the maximum load was determined from the derivative of the power law relation with respect to h (dP/dh). From the contact stiffness, the contact depth (the depth over which the indenter is in actual contact) was calculated using the relation as given by Equation 5.

$$h_c = h_{max} - 0.75\left(\frac{P_{max}}{S}\right) \tag{5}$$

The hardness and reduced elastic modulus (E_r) were determined as per the Equation 6 and 7.

$$H = \frac{P_{max}}{A} \tag{6}$$

$$E_r = \left(\frac{\sqrt{\pi}}{2\sqrt{A}}\right)S \tag{7}$$

where, A is the contact area in nm^2. The indentation hardness and the reduced elastic modulus at a P_{max} of 10 mN for each of the PECS samples are provided in Table 2. From the table, it can be inferred that an average hardness of ≈11 GPa and reduced elastic modulus of ≈95 GPa is exhibited by SiOC1500. In comparison, the hardness and reduced elastic modulus for fused quartz is ≈9 and ≈67 GPa, respectively. For understanding this variation better, the ratio of hardness to elastic

Table 2. Material properties of SiOC1300, SiOC1500 and fused quartz.

Sample	h_f/h_{max}	W_{el}/W_{tot}	H (GPa)	E_r (GPa)
SiOC1300	0.28 ± 0.02	0.71 ± 0.01	10.93 ± 0.89	106.18 ± 0.89
SiOC1500	0.31 ± 0.02	0.71 ± 0.01	10.97 ± 0.22	94.86 ± 1.36
Fused quartz	0.31 ± 0.01	0.76 ± 0.01	8.15 ± 0.16	67.40 ± 0.04

ADVANCED ENGINEERING MATERIALS 2013,
DOI: 10.1002/adem.201300146

ADVANCED ENGINEERING MATERIALS

modulus (H/E_r) is determined. H/E_r at a Pmax of 10 mN is ≈0.103, 0.116, and 0.134 for SiOC1300, SiOC1500, and fused quartz, respectively. This progressive increase in H/E_r ratio corresponds to the reduction in the elastic modulus with increase in the sintering temperature for the SiOC ceramics. The hardness values in these ceramics can be correlated to the silicon-oxycarbide tetrahedra, which are characterized by the presence of both covalent Si–C bonds and flexible Si–O–Si bonds. This substantiates that the presence of Si–C bond in the ceramic network results in exhibiting higher hardness than the fused quartz. Moreover, it can be inferred from Table 2 that the reduced elastic modulus decreased from ≈106 GPa for SiOC1300 to ≈95 GPa for SiOC1500. This drop in the modulus value can be correlated to the progressive phase separation of SiC and SiO_2 from the Si–O–C network thereby affecting the structural rigidity of the initial amorphous structure. Similar trend of decline in the modulus values with increase in heat-treatment temperature was also observed in Si–C–N[20] and Si–B–C–N[26] PDCs. Nevertheless, it is important to note that the hardness for SiOC1300 and SiOC1500 was closely similar (≈11 GPa) which could be correlated to the high density achieved at 1300 °C. Furthermore, the scatter observed in the indentation hardness was significantly lower for the PECS ceramics compared to any warm pressed and pyrolysed sample[29], indicating better homogeneity can be attained by PECS. However, the indentation hardness determined by micro-Vickers hardness was lower than that of nanoindentation hardness by a factor of ≈0.73 (Figure 5) which could be attributed to the possible difference in the load regimes considered.

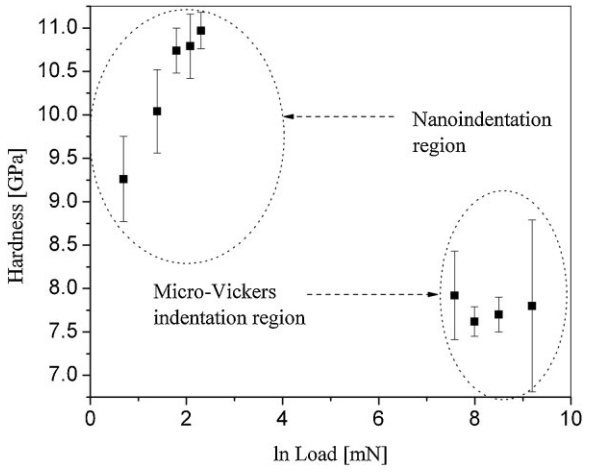

Fig. 5. Variation in hardness with ln (load) for SiOC1500.

The optical micrographs indicating the evolution of cracks upon indentation for SiOC1500 at indentation loads of 4900 and 9800 mN are shown in the Figure 6a–b. At 4900 mN, Hertzian cone cracks were observed for SiOC ceramics and with increase in the load to 9800 mN, these cone cracks tend to grow further outwards, with radius higher than the radius of indentation. Nevertheless, no substantial radial cracking was

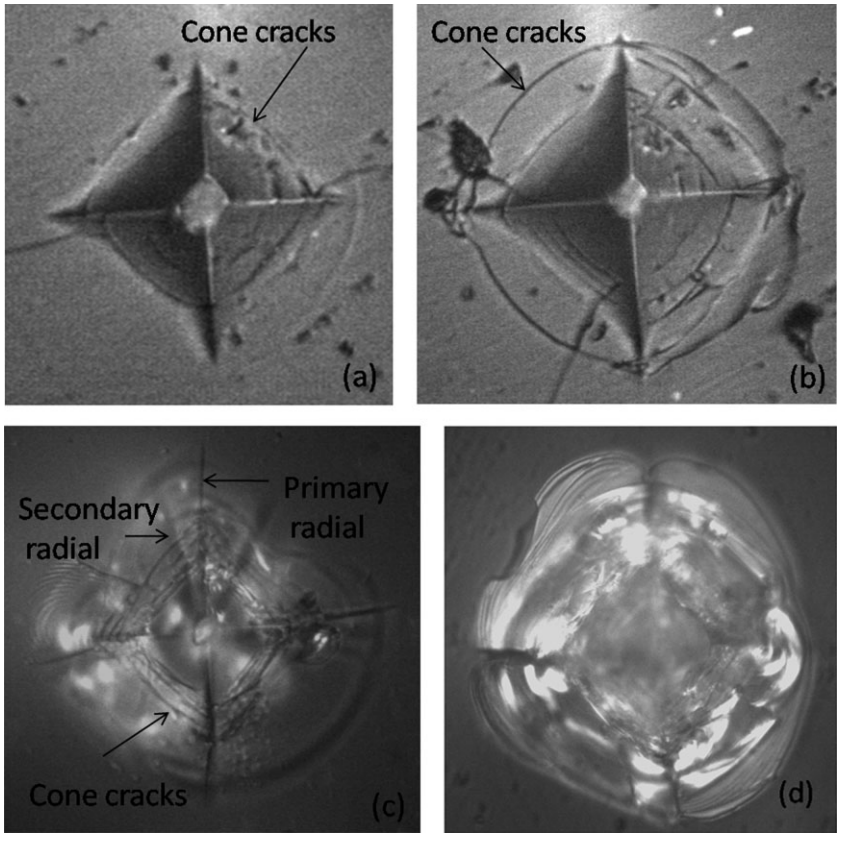

Fig. 6. Optical micrographs indicating the evolution of crack in PECS SiOC (a) at a P_{max} of 4900 mN; (b) at a P_{max} of 9800 mN and fused quartz ceramic (c) at a P_{max} of 4900 mN and (d) at a P_{max} of 9800 mN.

DOI: 10.1002/adem.201300146

observed. Hence, the evolution of the cracks in PECS SiOC can be considered analogous to the anomalous glasses, where deformation happens due to densification under the indentation. A similar anomalous densification behavior has been reported for the SiOC sol–gel derived glasses and was attributed to the flexibility of Si–O–Si bond.[30] Walter *et al*.[31] reported the existence of Hertzian conical cracks in the sol–gel derived SiOC samples thermolysed below 1000 °C and coexistence of conical and radial cracks above 1000 °C. The presence of cone cracks in fused quartz at an indentation load of 4900 mN is shown in Figure 6c. However, in addition to cone cracks, both primary and secondary radial cracks were also visible. Furthermore, upon loading at 9800 mN, these cone cracks tend to close (Figure 6d), whereas at similar loading conditions, the crack seem to be stable for SiOC1500 (Figure 6b). This suggests that the deformation mechanism observed in PECS SiOC though similar to that of fused quartz, the initiation of these crack sequences depends on the maximum indentation load[32] which in turn is a function of the type of bonds present in the material system. For that matter, the cracks produced in the SiOC ceramics can be considered to be more stable than fused silica because of the presence of stiffer Si–C bonds in former.

3. Conclusions

PECS was used for the production of SiOC PDCs and the ceramics were observed to undergo significant densification. The elastic constants determined from the non-destructive testing inferred that the values of these constants tend to show a marginal decrease with increase in sintering temperature. This was correlated to the phase evolution during sintering of these ceramics. The hardness and the elastic modulus determined by a depth sensing nanoindentation technique also exhibited a similar trend. The high elastic recovery displayed by these ceramics was in agreement with other PDCs subjected to contact loading. An elastic work ratio of ≈0.71 suggested that the determined hardness values were free of any significant pile-ups, which was further corroborated from the spanning probe micrograph. The presence of Hertzian cone cracks upon contact loading at 4900 and 9800 mN exemplified the anomalous deformation behavior. However, the evolution of these cracks was found to depend on the maximum indentation load.

Received: April 21, 2013
Final Version: June 10, 2013

[1] P. Colombo, G. Mera, R. Riedel, G. D. Soraru, *J. Am. Ceram. Soc.* **2010**, *93*, 1805.
[2] R. Riedel, G. Mera, R. Hauser, A. Klonczynski, *J. Ceram. Soc. Jpn.* **2006**, *114*, 425.
[3] M. Hojamberdiev, R. M. Prasad, K. Morita, M. A. Schiavon, R. Riedel, *Microporous Mesoporous Mater.* **2012**, *151*, 330.
[4] R. M. Prasad, A. Gurlo, R. Riedel, M. Hübner, N. Barsan, U. Weimar, *Sens. Actuat. B Chem.* **2010**, *149*, 105.
[5] N. Janakiraman, F. Aldinger, *J. Eur. Ceram. Soc.* **2009**, *29*, 163.
[6] S. Shah, R. Raj, *Acta Mater.* **2002**, *50*, 4093.
[7] R. Orrù, R. Licheri, A. M. Locci, A. Cincotti, G. Cao, *Mater. Sci. Eng. R.* **2009**, *63*, 127.
[8] Z. A. Munir, U. Anselmi-Tamburini, M. Ohyanagi, *J. Mater. Sci.* **2006**, *41*, 763.
[9] Z. A. Munir, D. V. Quach, M. Ohyanagi, *J. Am. Ceram. Soc.* **2011**, *94*, 1.
[10] J. Wan, M. J. Gasch, A. K. Mukherjee, *J. Am. Ceram. Soc.* **2002**, *86*, 526.
[11] M. Esfehanian, R. Oberacker, T. Fett, M. J. Hoffmann, *J. Am. Ceram. Soc.* **2008**, *91*, 3803.
[12] M. A. Mazo, C. Palencia, A. Nistal, F. Rubio, J. Rubio, J. L. Oteo, *J. Eur. Ceram. Soc.* **2012**, *32*, 3369.
[13] E. Radovanovic, M. F. Gozzi, M. C. Goncalves, I. V. P. Yoshida, *J. Non-Cryst. Sol.* **1999**, *248*, 37.
[14] Y. D. Blum, D. B. MacQueen, H.-J. Kleebe, *J. Eur. Ceram. Soc.* **2005**, *25*, 143.
[15] M. A. Schiavon, C. Gervais, F. Babonneau, G. D. Soraru, *J. Am. Ceram. Soc.* **2004**, *87*, 203.
[16] T. Rouxel, G. D. Soraru, J. Vicens, *J. Am. Ceram. Soc.* **2001**, *84*, 1052.
[17] A. A. El-Daly, F. El-Tantawy, A. E. Hammad, M. S. Gaafar, E. H. El-Mossalamy, A. A. Al-Ghamdi, *J. Alloy Compd.* **2011**, *509*, 7238.
[18] G. N. Greaves, A. L. Greer, R. S. Lakes, T. Rouxel, *Nat. Mater.* **2011**, *10*, 823.
[19] C. Moysan, R. Riedel, R. Harshe, T. Rouxel, F. Augereau, *J. Eur. Ceram. Soc.* **2007**, *27*, 397.
[20] N. Janakiraman, F. Aldinger, *J. Eur. Ceram. Soc.* **2010**, *30*, 775.
[21] R. Sujith, R. Kumar, *Ceram. Int.* **2013**, http://dx.doi.org/10.1016/j.ceramint.2013.04.095.
[22] A. A. El-Daly, M. Abdelhameed, M. Hashish, W. M. Daoush, *Mater. Sci. Eng. A* **2013**, *559*, 384.
[23] S. F. Pugh, *Phil. Mag.* **1954**, *45*, 823.
[24] W. C. Oliver, G. M. Pharr, *J. Mater. Res.* **1992**, *7*, 1564.
[25] W. C. Oliver, G. M. Pharr, *J. Mater. Res.* **2004**, *19*, 3.
[26] R. Sujith, R. Kumar, *J. Eur. Ceram. Soc.* **2013**, *33*, 2399.
[27] N. Iwashita, J. S. Field, M. V. Swain, *Phil. Mag. A* **2002**, *82*, 1873.
[28] M. Rodr guez, J. M. Molina-Aldaregu a, C. Gonz lez, J. L. Lorca, *Acta Mater.* **2012**, *60*, 3953.
[29] D. Galusek, F. L. Riley, R. Riedel, *J. Am. Ceram. Soc.* **2001**, *84*, 1164.
[30] T. Rouxel, J.-C. Sanglebœuf, J.-P. Guin, V. Keryvin, *J. Am. Ceram. Soc.* **2001**, *84*, 2220.
[31] S. Walter, G. D. Soraru, H. Bréquel, S. Enzo, *J. Eur. Ceram. Soc.* **2002**, *22*, 2389.
[32] R. F. Cook, G. M. Pharr, *J. Am. Ceram. Soc.* **1990**, *73*, 787.

DOI: 10.1002/adem.201300146